Finite-Element Analysis of Three-Dimensional Potential Flow in Turbomachines

Trifon E. Laskaris*
General Electric Corporate Research and Development, Schenectady, N. Y.

Because of the mathematical difficulties involved in the three-dimensional flow in turbomachinery cascades, present practice is to divide the problem into several coupled two-dimensional problems and construct from these a three-dimensional solution. For such problems, a finite-element technique is presented which is capable of solving the steady-state hydrodynamic equations of the three-dimensional compressible potential flow in rotating or stationary flow regions. The numerical algorithm is based on Galerkin's method applied over distorted curvilinear finite elements of the flow region where the absolute velocity potential is approximated by second-order Lagrange polynomials and nodal parameters. The process reduces the problem to a system of nonlinear algebraic equations which is solved by the Newton-Raphson iteration scheme. The method is applied to a mixed-flow type of turbine in subsonic flow of peak Mach number near unity. Equipotential lines and Mach number contours of the flowfield are presented. The pressure distribution on the blade surface discloses regions of steep pressure recovery where boundary-layer separation could occur.

Nomenclature

c_0 = $\hat{c}_0/U$, nondimensional velocity of sound at temperature T_0
e_n = finite element
F_{ijk} = element shape function at node ijk
H = $h + (V^2/2)$, nondimensional stagnation enthalpy
h = $\hat{h}/U^2$, nondimensional enthalpy
k = specific heat ratio of perfect gas
L = reference dimension
N_e = number of elements with common node ijk
P = $\hat{P}/P_0$, nondimensional pressure
P_0 = reference pressure
r = $\hat{r}/L$, nondimensional radius
S_n = surface of element e_n
S = $\hat{S}/U^2T_0$, nondimensional entropy
T_0 = reference temperature
T = $\hat{T}/T_0$, nondimensional temperature
u = $\hat{u}/U$, nondimensional radial velocity
U = reference velocity
v = $\hat{v}/U$, nondimensional absolute tangential velocity
V_n = volume of element e_n
V = $\hat{V}/U$, nondimensional absolute velocity vector
w = $\hat{w}/U$, nondimensional axial velocity
W = $\hat{W}/U$, nondimensional relative velocity vector
z = $\hat{z}/L$, nondimensional coordinate
α,β,γ = local coordinates
θ = coordinate
ρ = $\hat{\rho}/\rho_0$, nondimensional density
ρ_0 = reference density
ν = $\hat{\nu}/U$, nondimensional relative tangential velocity
Φ = $\hat{\Phi}/LU$, nondimensional absolute velocity potential
ω = $\hat{\omega}L/U$, nondimensional angular velocity

Superscript

$(\hat{\ })$ = dimensional quantity

Introduction

THE problem of three-dimensional flow in turbomachinery cascades has been the subject of considerable investigation in recent years. An early development of the theory of three-dimensional flow in subsonic and supersonic turbomachines was presented by Wu[1] as it pertains to turbomachines of axial-, radial-, and mixed-flow types with a finite number of thick blades.

Because of the mathematical difficulties involved in the problem, present practice[2,3] is to divide the problem into several coupled two-dimensional flow problems on stream surfaces and construct from these solutions a quasi-three-dimensional solution. One kind of stream surface considered is a blade-to-blade surface of revolution; the other kind identifies a stream surface that extends from the hub to the shroud and is typically midway between the blades.

A solution that is based on the coupling of these two-dimensional flow solutions is not strictly a solution of the three-dimensional flow problem, and the deviation from the true solution is not only difficult to evaluate but could also lead to significant discrepancies between the actual and predicted flow characteristics of a newly designed cascade.

To alleviate these problems, a finite-element technique is presented in this paper which is capable of solving the steady-state hydrodynamic equations of three-dimensional compressible potential flow in rotating or stationary flow regions. The numerical algorithm is based on the method of weighted residuals applied over distorted (often called isoparametric) finite elements of the flow region where the velocity potential is approximated by Lagrange polynomials and nodal parameters. Denton[4] approached the two-dimensional blade-to-blade potential flow problem by means of a time-marching method. The method can be extended to treat three-dimensional transonic flows.

Hydrodynamic Formulation

Consider the three-dimensional steady flow of a nonviscous, compressible fluid through a blade row rotating at constant angular velocity ω about the rotational axis. From the principles of conservation of matter, momentum, and energy, the equations of continuity and motion are written in nondimensional form as follows:

$$\nabla \cdot (\rho W) = 0 \tag{1}$$

$$-W \times (\nabla \times V) = -\nabla I + T\nabla S \tag{2}$$

Received Oct. 27, 1977; revision received Feb. 21, 1978.

Index categories: Computational Methods; Rotating Machinery.

*Acting Manager, Rotating Machinery Unit, Power Systems Laboratory.

where

$$I=h+(W^2/2)-(\omega^2 r^2/2)=H-\omega(vr) \tag{3}$$

If it is assumed that the fluid enters the inlet guide vanes of a turbomachine with a zero vorticity and uniform H and that the flow is isentropic, then, by virtue of Kelvin's circulation theorem, the absolute flow through the guide vanes will remain irrotational.

The guide vanes could impart a radial variation of tangential flow velocity downstream of the vanes, similar to that in a potential vortex. The fluid then enters the following rotor-blade row with zero vorticity of absolute flow, uniform H, uniform S, and, by virtue of Eq. (3), uniform I. Consequently, the absolute flow through the rotor-blade row can be treated as irrotational ($\nabla \times V=0$) and isentropic ($\nabla S=0$) with constant I throughout the cascade, according to Eq. (2). The equation of motion is reduced to

$$I-h-(V^2/2)+\omega(vr)=0 \tag{4}$$

The flow through the blade row is treated most conveniently by the use of an absolute velocity potential Φ, which is related to the relative velocity components by the expressions

$$\Phi_r=u, \quad \Phi_\theta/r=v=\nu+\omega r, \quad \Phi_z=w \tag{5}$$

For steady isentropic flow of a perfect gas, the density is related to the enthalpy by the nondimensional expression

$$\rho=\{[(k-1)/c_0^2]h\}^{1/(k-1)} \tag{6}$$

Equations (1) and (4-6) are sufficient to fully characterize the flow through the rotor-blade row.

The boundary-value problem of the flow through the rotor-blade row is defined in the flow region (Figs. 1-3) which rotates in unison with the rotor. The boundary conditions are prescribed as follows:

1) Inlet or outlet fluid boundaries. A potential distribution is prescribed by specifying the potential of one point on the fluid boundary and computing the potentials of the other points by means of uniform values of Φ_r, Φ_θ, and Φ_z. Uniform value of Φ_θ is required to generate a potential vortex whereby the absolute tangential velocity component v is inversely proportional to the radius. Thus, Dirichlet-type boundary conditions are applied only to the upstream and downstream fluid boundaries. The potential difference between the inlet and outlet fluid boundaries determines the flow rate through the region, provided that the flow is subsonic with local regions of supersonic flow.

2) Solid boundary. The relative velocity on the boundary surface must be tangent to the surface, namely, $(W\cdot n)=0$, where n is the normal unit vector to the surface.

3) Periodic boundary. The free surfaces of the blade upstream of the leading edges (C,D) and downstream of the trailing edges (E,F) are periodic boundaries of the blade row, where flow properties repeat themselves. The potential of a point on the free surface D or E must differ from the potential of the corresponding point on the free surface C or F by a fixed specified value. This boundary condition enforces continuity of the surface velocity vector on the periodic boundary but can only be applied to one of the free surfaces, say D or E. The boundary condition on the other free surface C or F then must satisfy continuity of the normal velocity vector on the periodic boundary. When both of these boundary conditions are satisfied, the absolute velocity vector is periodic, and so are all of the other flow properties. It should be pointed out that the periodic boundary condition also serves as the Kutta condition when applied to the leading edge, as well as the free surfaces E, F downstream of the leading edge.

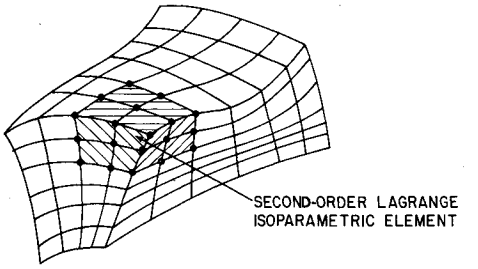

Fig. 1 Finite-element subdivision of fluid region.

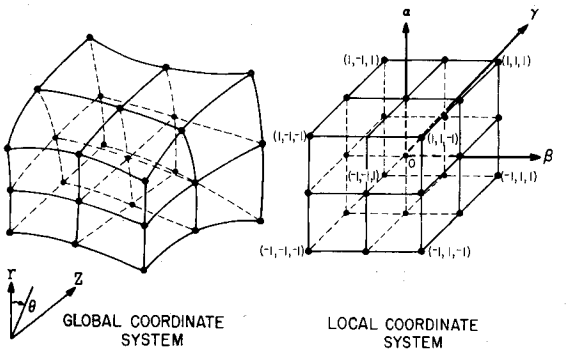

Fig. 2 Finite element in cylindrical and local coordinate system.

Finite-Element Weighted Residual Formulation

The flow region is subdivided into distorted finite elements of the second-order Lagrange family, as illustrated in Fig. 1. Let $r(\alpha,\beta,\gamma)$, $\theta(\alpha,\beta,\gamma)$, $z(\alpha,\beta,\gamma)$ be a one-to-one transformation of the distorted elements which yields cubes in the new coordinate system (α,β,γ) (see Fig. 2). It follows that

$$D(\alpha,\beta,\gamma)=\sum_{i=1}^{3}\sum_{j=1}^{3}\sum_{k=1}^{3}F_{ijk}(\alpha,\beta,\gamma)D_{ijk}$$

$$=\sum_{i=1}^{3}\sum_{j=1}^{3}\sum_{k=1}^{3}L_i(\alpha)L_j(\beta)L_k(\gamma)D_{ijk} \tag{7}$$

where D represents either r, θ, or z, and

$$L_1(x)=(x^2-x)/2, \quad L_2(x)=-(x^2-1),$$

$$L_3(x)=(x^2+x)/2$$

are the second-order Lagrange interpolation polynomials in the closed interval $(-1, 1)$. Note that the triple subscript ijk identifies the nodes of each element in the sense that the local coordinates of the node ijk are (i-2, j-2, k-2). A piecewise continuous representation of the absolute velocity potential Φ in terms of the functions $F_{ijk}(\alpha,\beta,\gamma)$ and the nodal parameters Φ_{ijk} is obtained from Eq. (7) by substituting Φ in place of D.

The method of weighted residuals is a general technique that can be used to reduce complex systems of partial differential equations to systems of algebraic equations which can be solved directly by standard numerical algorithms. An extensive application of the technique to two-dimensional viscous compressible and incompressible flow problems is presented by Laskaris.[5] A general discussion of the method of weighted residuals is given by Finlayson.[6] Galerkin's method, one of the weighted residual methods, is employed in the present investigation and is described in the following.

The continuity equation (1) is multiplied by the weighting function F_{ijk} of the node ijk and is integrated over the volume

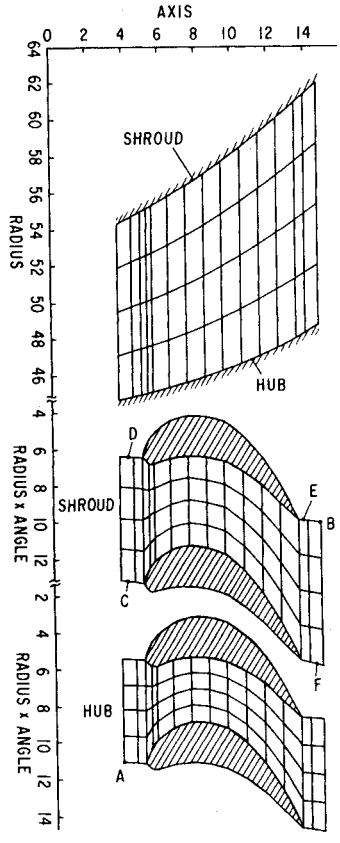

Fig. 3 Finite-element subdivision of flow region (in nondimensional coordinates) in rotor-blade row of a mixed-flow type of turbine.

V_n of the fluid element e_n to obtain

$$\int_{V_n} F_{ijk}\,\nabla\cdot(\rho \boldsymbol{W})\mathrm{d}V=\oint_{S_n} F_{ijk}\rho \boldsymbol{W}\cdot\boldsymbol{n}\mathrm{d}s$$

$$-\int_{V_n}\rho \boldsymbol{W}\cdot\nabla F_{ijk}\mathrm{d}V=0 \tag{8}$$

The density ρ can be expressed in terms of the absolute velocity components by means of Eqs. (4) and (6). The potential Φ is introduced in place of the velocity components, and Eq. (8) is written in nondimensional form as

$$\oint_{S_n} F_{ijk}\rho \boldsymbol{W}\cdot\boldsymbol{n}\mathrm{d}s-\int_{V_n}\left(\frac{k-1}{c_0^2}\right)^{1/(k-1)}\left[1+\omega\Phi_\theta\right.$$

$$\left.-\frac{1}{2}\left(\Phi_r^2+\frac{\Phi_\theta^2}{r^2}+\Phi_z^2\right)\right]^{1/(k-1)}\left[\Phi_r F_{rijk}+\left(\frac{\Phi_\theta}{r}-\omega r\right)\frac{F_{\theta ijk}}{r}\right.$$

$$\left.+\Phi_z F_{zijk}\right]r\,\mathrm{d}r\,\mathrm{d}\theta\,\mathrm{d}z=0 \tag{9}$$

When the polynomial approximation of the potential is substituted into Eq. (9), the left-hand side of the resulting expression represents the error due to the approximation in the subdomain of the element e_n.

The algebraic sum of all such contributions from the elements with common node ijk is set equal to zero to obtain, upon integration, the algebraic finite-element equation for the nodal parameter Φ_{ijk}. It follows that

$$\sum_{n=1}^{N_e}\left\{\int_{V_n}\left(\frac{k-1}{c_0^2}\right)^{1/(k-1)}\left[1+\omega\Phi_\theta-\frac{1}{2}\left(\Phi_r^2+\frac{\Phi_\theta^2}{r^2}+\Phi_z^2\right)\right]^{1/(k-1)}\right.$$

$$\left.\times\left[\Phi_r F_{rijk}+\left(\frac{\Phi_\theta}{r}-\omega r\right)\frac{F_{\theta ijk}}{r}+\Phi_z F_{zijk}\right]\times r\mathrm{d}r\,\mathrm{d}\theta\,\mathrm{d}z\right\}=0 \tag{10}$$

At internal nodal points, the closure integral term of Eq. (9) is assumed to have continuous integrand at the interelement boundaries. Thus, by assemblying the elements with common internal node ijk, the net closure integral vanishes:

$$\sum_{n=1}^{N_e}\oint_{S_n} F_{ijk}\rho \boldsymbol{W}\cdot\boldsymbol{n}\mathrm{d}s=0 \tag{11}$$

For that reason, Eq. (10) is strictly valid at interior nodes.

At points of a solid boundary surface, the velocity vector $\boldsymbol{W}$ is tangent to the surface ($\boldsymbol{W}\cdot\boldsymbol{n}=0$), Eq. (11) is still valid, and Eq. (10) is the appropriate boundary condition. The integral of Eq. (10) can be evaluated most conveniently in the local coordinate system (α,β,γ), where explicit relations for the Lagrange interpolation polynomials are available readily. Thus, it is required to express all derivatives of the integrand in the local coordinate system. The task is carried out using the partial differential operators

$$\frac{\partial}{\partial r}=\frac{1}{J}\left[(\theta_\beta z_\gamma-z_\beta\theta_\gamma)\frac{\partial}{\partial\alpha}+(z_\alpha\theta_\gamma-\theta_\alpha z_\gamma)\frac{\partial}{\partial\beta}\right.$$

$$\left.+(\theta_\alpha z_\beta-z_\alpha\theta_\beta)\frac{\partial}{\partial\gamma}\right] \tag{12a}$$

$$\frac{\partial}{\partial\theta}=\frac{1}{J}\left[(z_\beta r_\gamma-r_\beta z_\gamma)\frac{\partial}{\partial\alpha}+(r_\alpha z_\gamma-z_\alpha r_\gamma)\frac{\partial}{\partial\beta}\right.$$

$$\left.+(z_\alpha r_\beta-r_\alpha z_\beta)\frac{\partial}{\partial\gamma}\right] \tag{12b}$$

$$\frac{\partial}{\partial z}=\frac{1}{J}\left[(r_\beta\theta_\gamma-\theta_\beta r_\gamma)\frac{\partial}{\partial\alpha}+(\theta_\alpha r_\gamma-r_\alpha\theta_\gamma)\frac{\partial}{\partial\beta}\right.$$

$$\left.+(r_\alpha\theta_\beta-\theta_\alpha r_\beta)\frac{\partial}{\partial\gamma}\right] \tag{12c}$$

where J is the Jacobian of the coordinate transformation, written as

$$J=r_\alpha(\theta_\beta z_\gamma-z_\beta\theta_\gamma)+\theta_\alpha(z_\beta r_\gamma-r_\beta z_\gamma)+z_\alpha(r_\alpha\theta_\gamma-\theta_\beta r_\gamma) \tag{13}$$

Because of the nonlinearity of the integral equation (10), the nodal parameters at each node can only be related implicitly to the nodal parameters of the neighborhood nodes. Let $\boldsymbol{\Phi}=(\Phi_1,\Phi_2,\ldots,\Phi_N)$ stand for the vector of the unknown potentials, and

$$\int_V\psi_j(\boldsymbol{\Phi})\mathrm{d}V=0,\quad j=1,2,\ldots,N \tag{14}$$

be an abreviated form of the system of Eqs. (10). The Newton-Raphson iteration scheme can be employed to solve the nonlinear system of Eqs. (14). The iteration scheme provides a correction vector $\boldsymbol{\Omega}^k$ at the kth iteration which is defined as the solution vector of the linear system of equations

$$\sum_{i=1}^{N}\left[\int_V\left(\frac{\partial\psi_j}{\partial\Phi_i}\right)_{k-1}\mathrm{d}V\right]\Omega_i^k$$

$$=-\int_V\psi_j(\boldsymbol{\Phi}^{k-1})\mathrm{d}V,\quad j=1,2,\ldots,N \tag{15}$$

The correction vector $\boldsymbol{\Omega}^k$ is added to the vector $\boldsymbol{\Phi}^{k-1}$ of the $(k-1)$th iteration to give a better approximation $\boldsymbol{\Phi}^k=\boldsymbol{\Phi}^{k-1}+\boldsymbol{\Omega}^k$ to the solution of the system of Eqs. (14). Convergence is reached when the components of the correction vector $\boldsymbol{\Omega}^k$

are at least five orders of magnitude smaller than the corresponding components of the solution vector Φ^{k-1}. The system of Eqs. (15) has a nonsymmetric, banded coefficient matrix. The solution is obtained by the well-known Gauss elimination and resubstitution technique, taking into full account the sparceness of the equations to shorten the computation time.

To accelerate the convergence of the iteration scheme, it is recommended to start the iteration with the solution of the linear system of equations

$$\sum_{n=1}^{N_e} \int_{V_n} \left[\Phi_r F_{rijk} + \left(\frac{\Phi_\theta}{r} - \omega r \right) \frac{F_{\theta ijk}}{r} + \Phi_{zijk} F_{zijk} \right] r \, dr \, d\theta \, dz = 0 \tag{16}$$

subject to the same boundary conditions. In other words, the first approximation to the compressible flow problem is the solution to the incompressible flow problem.

It is evident from the preceding that an attempt to formulate the integral expression of Eq. (10) explicitly would lead to a formidable task. Numerical integration, on the other hand, is best suited for integration of polynomials. A Gaussian quadrature scheme,[7] for example, using $n \times n \times n$ sampling points will exactly integrate all polynomial expressions of the form $\Sigma C_{ijk} \alpha^i \beta^j \gamma^k$, where $i,j,k \leqq 2n-1$. In the present investigation, a Gaussian quadrature of $3 \times 3 \times 3$ points is employed to evaluate the integrals of Eq. (15).

Application to a Rotor-Blade Row

The application of the method to a specific rotor-blade row configuration discussed here aims to demonstrate the capability and efficiency of the method in analyzing a truly three-dimensional compressible flowfield, study the stability of the iteration scheme, and gain insight into the physical interpretation of the solution. In that respect, the rotor-blade row configuration was selected arbitrarily, as illustrated in Fig. 3, to be representative of a mixed-flow type of turbomachine, having significant amounts of flow in both the axial and radial directions. The input data for the case studied are summarized in Table 1.

The finite-element grid size often is selected from conflicting considerations of accuracy, resolution of the flowfield, and computation time. Design optimization of a new blade-row geometry, for example, requires repeated computations of the three-dimensional flowfield. It is desirable, therefore, to carry out the optimization process with a coarse finite-element grid, which is capable of generating inexpensive but fairly accurate solutions. When the blade geometry is optimized, a finer grid is employed to resolve detail and improve the accuracy of the solution.

The flow region of Fig. 1 is subdivided into finite elements using two grid sizes namely, a coarse grid of $5 \times 5 \times 15$ nodal points and a finer grid of $5 \times 9 \times 29$ nodal points that comprises the coarse grid with the addition of midpoint grid subdivisions on blade-to-blade surfaces of revolution. Computation of the flowfield is carried out with both grids to evaluate the computational time and relative accuracy of the solutions. The mean value of the absolute fractional deviation of the potential,

$$\epsilon = \frac{1}{N} \sum_{i=1}^{N} \left| \frac{\Delta \Phi_i}{\Phi_i} \right|$$

is used to assess the relative accuracy of the solutions.

In this investigation, a General Electric 605 digital computing system is used to perform the numerical computations. An initial estimate of the potential field is generated by solving Laplace's equation for potential incompressible flow. Subsequently, the Newton-Raphson iteration scheme is carried out to reach convergence in two iterations. The potential field is used to compute, at each nodal point, the absolute velocity vector components, the Mach number, the pressure, and the density. Because of discontinuity of the derivatives at the interelement boundaries, a mean derivative is computed by averaging contributions from all elements with common nodal points.

Table 1 Specification of flow characteristics

Characteristic	Specification
Perfect gas	Air
Angular velocity $\hat{\omega}$, 1/s	377
Reference quantities	
Dimension L, m	0.01
Velocity, U, m/s	100
Density ρ_0, kg/m^3	3.484
Temperature T_0, K	1000
Pressure P_0, N/m^2	10^6
Stagnation properties	
Density ρ_s, kg/m^3	4.002
Temperature T_s, K	1057
Pressure P_s, N/m^2	1.214×10^6
Inlet flow	
Radial velocity $\hat{u}$, m/s	70
Tangential velocity $\hat{v}$, m/s, over radius $\hat{r}$, m	$140/\hat{r}$
Potential $\hat{\Phi}$, m^2/s, at point A (Fig. 3)	0
Outlet flow	
Radial velocity $\hat{u}$, m/s	140
Tangential velocity $\hat{v}$, m/s, over radius $\hat{r}$, m	$97/\hat{r}$
Potential $\hat{\Phi}$, m^2/s, at point B (Fig. 3)	55

The computation time in the General Electric 605 computer, a relatively slow model, is typically 20 min for the coarse grid and 160 min for the finer grid. The improvement in accuracy achieved with the finer grid is only $\epsilon = 0.86\%$. Consequently, for all practical purposes, the coarse grid yields results about as accurate as the finer grid at a considerably shorter computation time and will be used as the basis in the following discussion.

Equipotential surfaces provide a useful representation of the flowfield, since the streamlines of the absolute flow are perpendicular to the equipotential surfaces. Figure 4 displays, in a developed view, the lines of intersection of the equipotential surfaces with two surfaces of the finite-element grid, namely, the hub and the shroud. It is worth noting that the equipotential surfaces are not perpendicular to the blade surface, since the absolute velocity is not tangent to the blade surface.

At the pressure side of the blade, near the trailing edge the potential field discloses a stagnation point. The stagnation point is slightly upstream of the trailing edge on the hub and virtually coincides with the trailing edge at surfaces of revolution approaching the shroud. The presence of a stagnation point near the trailing edge insures that the streamlines are attached to the trailing edge rather than detached from it. The latter condition could result in unrealistically large calculated velocities near the trailing edge.

The throughflow problem is best illustrated in Fig. 5, which is an azimuthal projection of a grid surface midway between two blades on a meridian. Strictly speaking, the projections of the equipotential lines meet with the hub and shroud boundaries at right angles only when the grid surface is radial. This is clearly the case with the radial sections of the grid surface upstream and downstream of the blade row.

Mach number contours are of considerable interest in compressible flow studies inasmuch as they represent a measure of the magnitude of the velocity vector against the local velocity of sound and depict compressibility phenomena

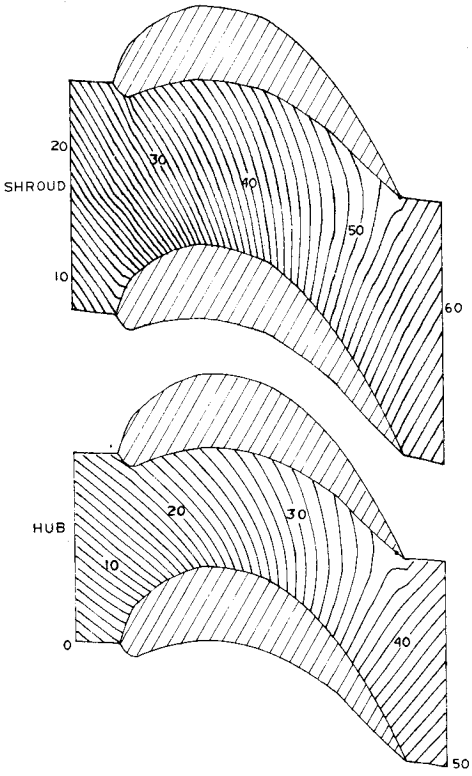

Fig. 4 Equipotential lines on blade-to-blade surfaces of revolution.

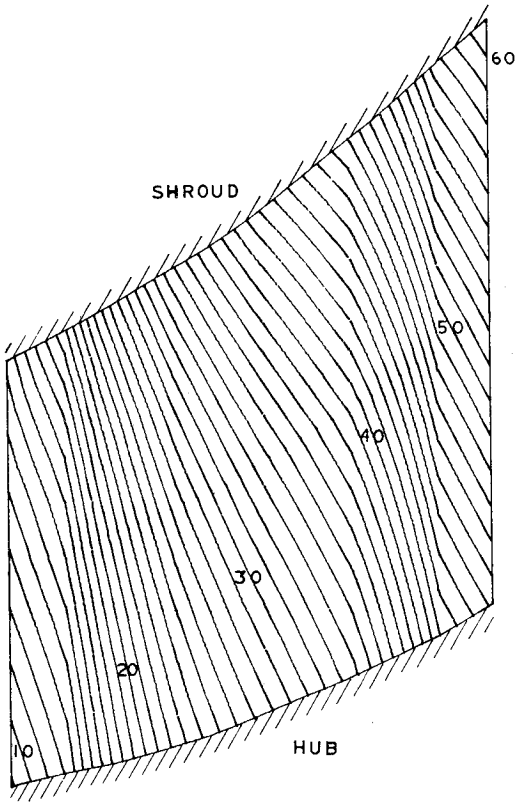

Fig. 5 Equipotential lines on surface midway between two blades.

such as choking, shock waves, etc. As before, the Mach number contours are plotted in Fig. 6 on a developed view of the hub and the shroud. The Mach number contours on these surfaces of revolution have a common characteristic similarity. They all depict a rapid acceleration of the gas at the pressure side of the blade near the leading edge and a slower

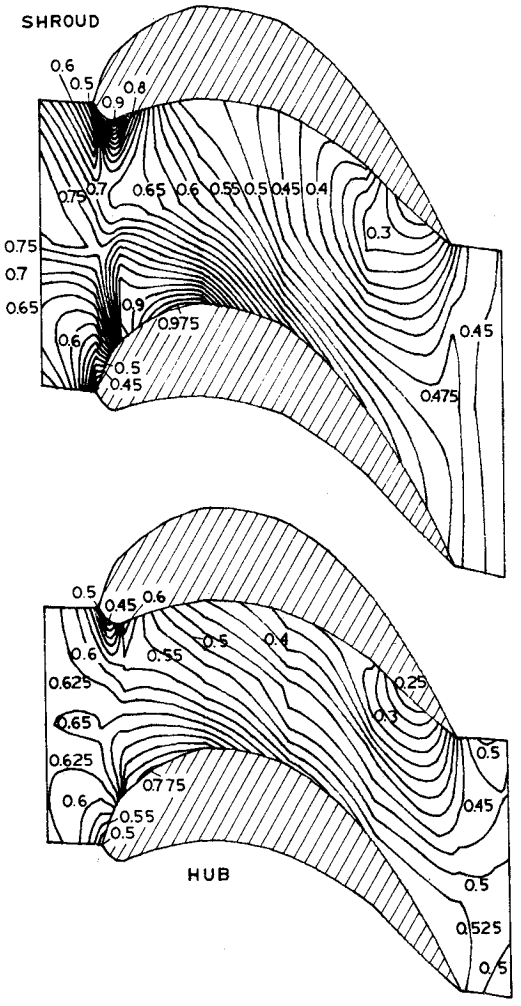

Fig. 6 Mach number contours on blade-to-blade surfaces of revolution.

acceleration at the suction side of the blade, with the maximum Mach number always occurring on the suction side of the blade.

Inspection of the Mach contours of Fig. 6 further indicates that the maximum Mach number on surfaces of revolution increases progressively from 0.77 at the hub to 0.98 at the shroud, whereas the point where the peak occurs shifts slightly downstream along the suction side of the blade. The radial profiles of Mach number are illustrated best in Fig. 7, where the Mach number contours are plotted on the grid surface halfway between the blades.

Another important result in Fig. 6 is the fact that choking initiates on the shroud and suction side of the blades, where the peak Mach number is near unity. The reason for the higher Mach numbers in the shroud region is the higher tangential velocity of the blade tip.

Local regions of supersonic flow were present in some of the cases studied; however, the majority of the flowfield was subsonic. In other words, the elliptic behavior of the flow was not disturbed by the presence of local regions of hyperbolic behavior. On the other hand, the present boundary conditions are not suitable for handling transonic flow cases where supersonic flow prevails, because Dirichlet-type boundary conditions on both upstream and downstream boundaries are inconsistent with the hyperbolic behavior of supersonic flow.

Additional insight into the flow may be obtained by studying the pressure profiles. The pressure profiles on the blade surface not only give the net force on the blade but also throw light on the occurrence of boundary-layer separation in regions with steep adverse pressure gradients.

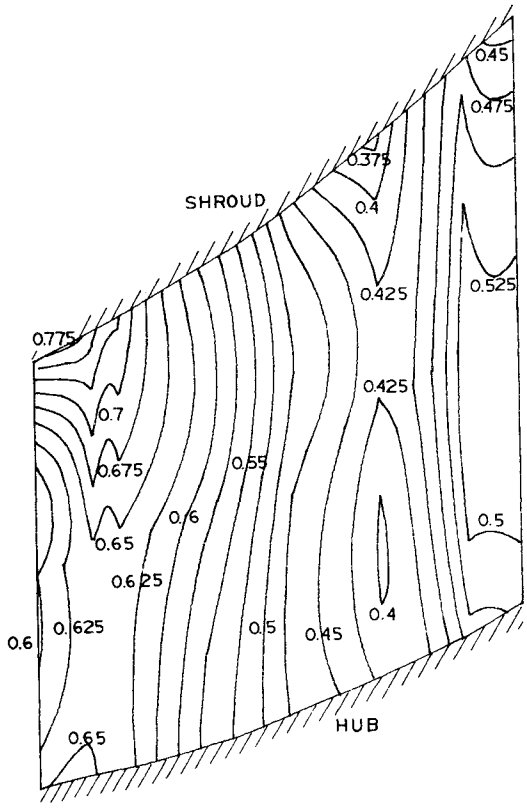

Fig. 7 Mach number contours on surface midway between two blades.

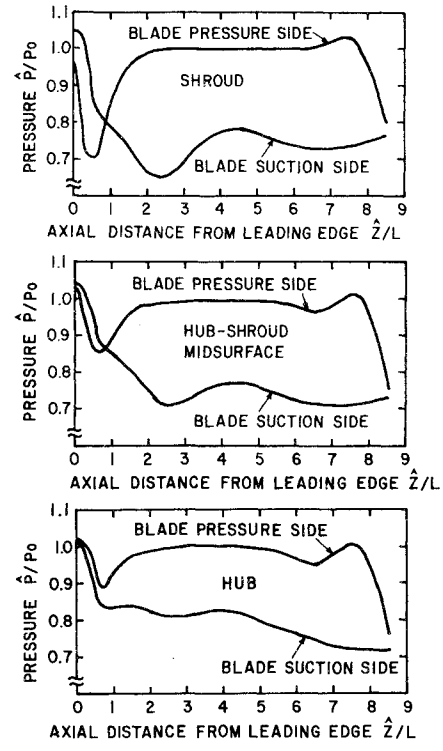

Fig. 8 Pressure distribution on the blade surface.

Shown in Fig. 8 are the pressure distribution curves at the intersections of the blade surface with three surfaces of revolution, namely, the hub, the shroud, and the surface midway between the hub and the shroud. The pressure profiles on the suction side of the blade generally are characterized by sharp and moderate pressure drops downstream of the leading edge, followed by a slight or no pressure recovery. A sharp pressure drop also occurs at the pressure side of the blade near the leading edge, but it is followed by a pressure recovery nearly as strong. Immediately thereafter, the pressure remains nearly constant over most of the blade surface, and a second steep pressure drop occurs just upstream of the trailing edge.

The pressure drop and recovery at the pressure side of the blade near the shroud result from the unfavorable blade geometry with regard to the inlet flow direction. It is apparent that no adjustment was made on the blade geometry to account for the radial variation of the inlet flow angle. A thinner plate near the leading edge, for example, also could help to smooth these pressure gradients.

One of the most important points to be made in connection with Fig. 8 is that the steep pressure recovery on the shroud predicted by the inviscid flow computation inevitably will bring about boundary-layer separation of the viscous flow and will result in only partial pressure recovery. Loss of power by virtue of boundary-layer separation is a well-known consequence of such nonoptimum blade designs. Accurate prediction of the three-dimensional pressure distribution of a newly designed blade configuration enables one to improve the design so as to reduce inefficiencies caused by boundary-layer separation.

Concluding Remarks

The preceding describes the development of a finite-element technique that is capable of solving the steady-state hydrodynamic equations of three-dimensional compressible potential flow in rotating or stationary flow regions, in general, and specifically in rotor and stator cascades of turbomachines. The finite-element algorithm makes use of distorted curvilinear elements of the second-order Lagrange family to approximate the absolute velocity potential in terms of nodal parameters and polynomial functions. Galerkin's method, one of the weighted residual methods, is employed to reduce the hydrodynamic equations to a system of nonlinear algebraic equations for the nodal parameters. A stable solution is obtained by means of the Newton-Raphson iteration scheme. Numerical integration is used to evaluate the coefficients of the Jacobian matrix and the source vector in each iteration.

The method is applied to a rotor-blade row configuration of a mixed-flow type of turbine in subsonic flow of peak Mach number near unity. Equipotential lines and Mach number contours of the computed flowfield are presented on blade-to-blade surfaces of revolution, as well as on the surface midway between the blades. The pressure distribution on the blade surface discloses regions of steep pressure recovery where boundary-layer separation could occur. The method can be implemented efficiently to improve the design of a new rotor or stator blade-row configuration so as to reduce boundary-layer separation.

References

[1] Wu, C. H., "A General Theory of Three-Dimensional Flow in Subsonic and Supersonic Turbomachines of Axial-, Radial, and Mixed-Flow Types," NACA TN 2604, Jan. 1952.

[2] Katsanis, T., "Fortran Program for Calculating Transonic Velocities on a Blade-to-Blade Stream Surface of a Turbomachine," NACA TN D-5427, Sept. 1969.

[3] Prince, T., "Prediction of Transonic Inviscid Steady Flow in Cascades by Finite Element Methods," Ph.D. dissertation, Univ. of Cincinnati, 1976.

[4] Denton, J., "A Time Marching Method for Two and Three Dimensional Blade to Blade Flows," Aeronautical Research Council, R&M 3775, Oct. 1974.

[5] Laskaris, T. E., "Finite-Element Analysis of Compressible and Incompressible Viscous Flow and Heat Transfer Problems," *The Physics of Fluids*, Vol. 18, Dec. 1975, p. 1639.

[6] Finlayson, B. A., *The Method of Weighted Residuals and Variational Principles*, Academic Press, New York, 1972.

[7] Stroud, A. H. and Secrest, D., *Gaussian Quadrature Formulas*, Prentice-Hall, Englewood Cliffs, N.J., 1966, p. 100.